Effect of Cu doping concentration on H$_2$S gas-sensing properties of Cu-doped SnO$_2$ thin films

Pankaj S. Kolhe[1] · Sunil G. Kulkarni[1] · Namita Maiti[2] · Kishor M. Sonawane[1]

Abstract

Metal oxide-based gas sensors doped with metal element have attracted many researchers due to their enhancement in physico-chemical properties as compared to pristine counterpart. Herein, a novel idea of tailoring the structure and properties by controlling the doping percentage is used to obtain the optimum performance characteristics. The present communication reports synthesis of pristine SnO$_2$ and in situ Cu-doped SnO$_2$ films using simple chemical spray pyrolysis technique to study H$_2$S gas-sensing characteristics. The synthesized pristine and Cu-doped SnO$_2$ films were characterized using X-ray diffraction (XRD), scanning electron microscopy (SEM) and UV–visible spectroscopy to reveal their structural, morphological, and optical properties, respectively. To ascertain the presence of CuO/SnO$_2$ interface, transmission electron microscopy (TEM) is carried out. Optimum doping concentration and operating temperature is determined by studying the gas-response characteristics for various doping concentrations at different operating temperatures. For this combination of optimum doping concentration and operating temperature, repeatability as well as response and recovery time towards H$_2$S gas are systematically studied.

1 Introduction

Metal oxide semiconductors have attracted more attention of researches in recent time because of their excellent physico-chemical properties and become potential candidates to find the application in various fields such as electronic, optical, optoelectronic fields [1]. Particularly, SnO$_2$, ZnO, and TiO$_2$ which possess a wide energy bandgap, tremendous electrical conductivity and optical transparency make them vital materials in field of electronic devices [2]. Among the variety of metal oxide semiconductors, Tin dioxide (SnO$_2$) is acknowledged as one of the suitable material for multifunctional applications. The excellent chemical, electrical properties and wide bandgap (3.6 eV), native oxygen vacancies and high carrier density of SnO$_2$ are the main reason of being a potential material to be used in solar cell, lithium-ion rechargeable batteries, field emitter and gas sensor applications [3–5]. Moreover, SnO$_2$ is cost effective, physically stable and can be operated at wide range of temperatures; therefore it becomes most reliable material in field of gas sensing to detect and monitor variety of pollutant and toxic gases such as CO, NH$_3$, H$_2$S etc. [6–8].

As a known fact, hydrogen sulfide (H$_2$S) is highly toxic, bad smelling; flammable gas, can cause irritation to respiratory tract, nausea and is dangerous to human health. It is produced as a by-product in laboratories and pharmaceutical industry. Above 250 ppm level, the H$_2$S gas can cause neurobehavioral toxicity and may even cause death [9]. Therefore, much attention has been given to detect H$_2$S gas. However, SnO$_2$ as a gas sensor has encountered by many drawbacks such as slow response, low sensitivity and very high operating temperatures. To improve the gas-sensing performance of the sensor, researchers have functionalized the SnO$_2$. For that purpose several approaches have been employed such as decorating SnO$_2$ nanostructure with metal particle [10, 11], forming nanocomposite with other metal oxide semiconductor [12, 13]. Doping metallic element impurities such as Ni, Pd, Ru, Cu etc. into SnO$_2$ is regarded as an effective approach to tailor the electronic properties

✉ Kishor M. Sonawane
kmsonawane@gmail.com

[1] Deparment of Physics, Fergusson College Affiliated Savitribai Phule Pune University, Pune 411004, India

[2] Laser and Plasma Technology Division, Bhabha Atomic Research Centre, Trombay, Mumbai 400 085, India

and provides more gas adsorption-active sites for gas sensing thereby improving sensing performance of SnO_2-based gas sensor [14–16]. Among the numerous metallic dopants, Cu has favored as an important one, because it increases the formation of surface-oxygen vacancies in SnO_2, which are essential to facilitate the adsorption of oxygen ion species on the surface of SnO_2 [17]. Bhardwaj et al. reported facile wet chemical method to prepare Cu-doped SnO_2 nanostructure which shows highly enhanced and excellent selectivity for CO gas due to Cu doping [18]. The influence of Cu doping on formaldehyde gas sensing property of SnO_2 nanoparticles was reported by Mishra et al. [19]. Authors reported that, the magnitude of sensitivity is higher than that of undoped SnO_2. Liu et al. reported improved ethanol sensing of SnO_2 due to Cu doping. In which, authors investigated that the sensitivity of Cu-doped sensor was raised to six times more than the undoped SnO_2 sensor [20]. Ghimbeu et al. reported, electrostatic spray deposition of Cu-doped SnO_2 film for H_2S gas detection. The films showed the low level detection of H_2S gas at temperature of 100 °C [21]. Effect of post thermal treatment on gas sensing characteristics of Ag–SnO_2 nanocomposite towards CO gas was studied by Bhardwaj et al. [22]. It was observed that, sensor fabricated using annealed Ag–SnO_2 nanocomposite exhibits enhanced sensor response as compared to as-deposited sensor.

Incorporation of CuO in SnO_2 is reported to create oxygen vacancies which give rise to active sites useful for enhancing the gas-sensing characteristics. The interface of CuO/SnO_2 wherein the Sn is substituted by Cu deems to be responsible for enhancement in sensing characteristics. Thus, it is required that, the optimum doping percentage of Cu needs to be determined for which the maximum amount of CuO will enter into the basic lattice of SnO_2 giving rise to maximum number of active sites. It is envisaged that, at very low doping concentrations the CuO instead of entering into the lattice will form thin layers on the grain boundaries. With the increase in doping concentration more and more CuO will start entering into the lattice till the solubility limit is exceeded. Beyond this doping concentration the CuO will have a tendency of forming agglomeration on grain boundaries instead of going into the lattice. These studies will help in finding the optimum doping concentration that will give rise to maximum number of active sites and thereby maximum gas response. With this hypothesis, the present communication reports, the synthesis of pristine and in situ Cu-doped SnO_2 thin films for the doping concentration of Cu ranging from 0.006 to 0.014 M with step of 0.002 M by facile spray pyrolysis technique.

The objective of the present study is to tailor the structure of synthesized material that will give rise to maximum performance characteristics. The estimate of correct doping concentration that will give rise to the desires structural parameters is done by varying doping concentration from a very low level to the level wherein the solubility limit is exceeded so as to give exact value of the optimum doping concentration. In this regards the structural, morphological, optical and H_2S gas-sensing properties of pristine and Cu-doped SnO_2 thin film have been studied. The results showed that, as per the hypothesis, incorporation of Cu modifies structural as well as optical properties of host SnO_2 material. The Cu-doped SnO_2 sensors have shown enhanced response to H_2S gas with fast and moderate response and recovery times, respectively. It indicates that Cu-doped SnO_2 sensor would have potential application in H_2S gas detection.
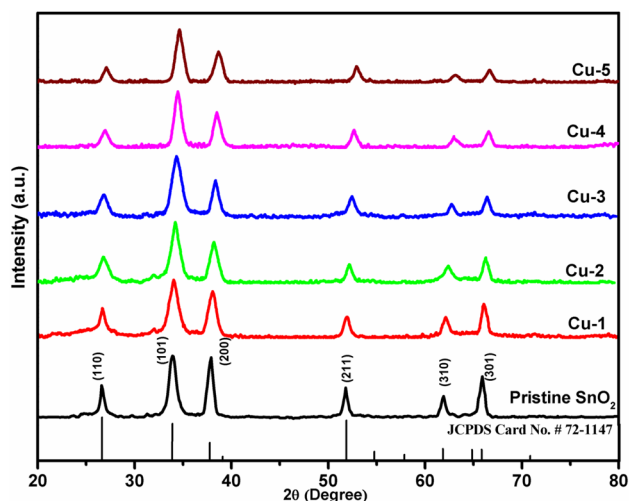
2 Experimental

2.1 Synthesis of pristine SnO₂ and Cu-doped SnO₂ thin films

Tin oxide (SnO_2) thin films have been deposited on glass substrate (microscopic glass slide) by spray pyrolysis technique using the precursor solution, prepared by dissolving 0.2 M of $SnCl_4·5H_2O$ in mixture of three parts of methanol and one part of distilled water, i.e., (3:1 proportion) [8, 23]. Copper chloride di-hydrated ($CuCl_2·2H_2O$) of concentration varying from 0.006 to 0.014 M with step of 0.002 M has been used as a Cu dopant source for Cu-doped SnO_2 thin film and referred as "Pristine SnO_2", "Cu-1", "Cu-2", "Cu-3", "Cu-4" and "Cu-5", respectively, in further part of present communication. The prepared precursor solution of 35 ml was sprayed with flow rate 3.5 ml/min using air as carrier gas on preheated glass substrate which was maintained at temperature 420 °C. The deposited films were allowed to cool naturally on the heater surface. All the films were annealed at temperature 450 °C in PID-controlled muffle furnace for 2 h for better crystallinity and adhesion.

2.2 Characterization and gas-sensing study

For structural study of as-deposited pristine SnO_2 and Cu-doped SnO_2 thin films were examined by X-ray diffraction (XRD, D8 Advance, Bruker AXS) using Cu Kα radiation of 1.543 Å. The surface morphology of the films was studied using scanning electron microscopy (SEM, JEOL, JSM-6360A). The optical properties of all the thin films were carried out using UV–visible spectroscopy (JASCO 760). The Tauc plot graph is plotted using data of UV–visible spectroscopy to find out the optical band gap.

The gas-sensing performance of the films was studied using two-probe method, the detailed method is discussed elsewhere [24]. The gas-sensing study was performed using standard two-probe sensing system, which involves stainless steel chamber equipped with electrical feedthroughs and gas inlet port. All the measurements of gas sensing

Fig. 1 XRD patterns of pristine SnO_2 and Cu-doped SnO_2 films

Table 1 The lattice constant values of undoped and Cu-doped SnO_2 thin films

Sr. no.	Sample	Copper (Cu) concentration (M)	Lattice parameter (Å)	
			(a = b)	(c)
1	Pristine SnO₂	0	4.73352	3.18387
2	Cu-1	0.006	4.71958	3.18175
3	Cu-2	0.008	4.70573	3.18266
4	Cu-3	0.010	4.69367	3.18541
5	Cu-4	0.012	4.68316	3.19898
6	Cu-5	0.014	4.6762	3.20315

characteristics such as response and recovery were carried out in static mode. The H₂S gas-sensing characteristics at different temperature and different concentration were recorded using a Keithley 2450 6½ digital multimeter-cum-source meter. Initially, the response of all the films for fixed concentration of gas at different temperatures from room temperature (RT) to 300 °C is recorded. After optimizing the operating temperature (150 °C) for gas sensing, the characteristics like response and recovery time and response at various concentrations of H₂S gas were investigated. The response of the sensor can be defined as,

$$S(\%) = \left(\frac{R_a - R_g}{R_a} \right) \times 100, \tag{1}$$

where R_a and R_g are the resistances of the sensor in the air and the target gas, respectively.

3 Results and discussion

3.1 Structural analysis

The structural parameters and purity of phase are obtained from XRD diffraction patterns. The XRD pattern of as-deposited pristine SnO₂ and Cu-doped SnO₂ thin films are shown in Fig. 1. All the obtained diffraction peaks are well indexed to tetragonal structure of rutile phase of SnO₂ and are in good agreement with the reported values from JCPDS Card No. 72-1147 (a = 4.737 Å and c = 3.185 Å) [25]. Considering the signal-to-noise ratio over the entire span of values of 2θ from 20° to 80°, the peaks with very low values of this ratio are not indexed and taken into consideration. Only the prominent peaks with considerable values of $I/I_{\max}$.

are indexed and taken to consideration. Figure 1 reveals the intensity of diffraction peaks is observed to decrease with the increasing Cu concentration which indicates that the crystallinity of SnO₂ deteriorates. This can be attributed to the fact that, the host SnO₂ system enables more nucleation sites with the incorporation of Cu in it, which limits the growth of crystal grains resulting in deterioration of crystallinity [19]. Moreover, it is observed that the diffraction peaks of Cu-doped SnO₂ films are slightly shifted to higher diffraction angle in comparison with the pristine SnO₂. Consequently, the lattice parameters have been found to vary from the standard values (a = 4.737 Å and c = 3.185 Å). The observed values of lattice parameters 'a' and 'c' for pristine SnO₂, Cu-1, Cu-2, Cu-3, Cu-4 and Cu-5 are shown in the Table 1.

Due to incorporation of Cu ion into SnO₂ lattice, actually the size of the lattice and hence 'a' values should go on increasing. However, Cu^{2+} has much higher electron negativity than Sn^{4+}, therefore, it exerts much larger force of attraction on O^{2-} ions which results into overall shrinkage of the lattice. This can be observed in Table 1, as the values of 'a' decrease with increase in Cu doping. The deviation in lattice parameters values can be attributed to the incorporation of Cu^{2+} ions into the SnO₂ lattice. The ionic radii of Sn^{4+} and Cu^{2+} are 0.069 nm and 0.073 nm, respectively, which seem to be comparable. As result of this the substitution mechanism is dominant in the incorporation of Cu^{2+} ions into SnO₂ lattice network [19, 26]. The Cu^{2+} ions which substitute Sn^{4+} ions of SnO₂ lattice, cause the variation in lattice parameter values.

The Williamson–Hall (W–H) plot was constructed with $\beta\cos\theta/\lambda$ versus $\sin\theta/\lambda$ for pristine SnO₂ and Cu-doped SnO₂ films are shown in supporting information (SI Fig. 1). The W–H plot interprets strain on the lattice as well as crystallite size of the sample is shown in Table 2.

Table 2 Strain and crystallite size of pristine and Cu-doped SnO_2 thin films

Sample name	Strain	Crystallite size (nm) From W–H plot	Crystallite size (nm) From Debye–Scherrer
Pristine SnO_2	− 0.01246	9.18	9.36
Cu-1	− 0.00852	8.96	9.04
Cu-2	− 0.02849	6.34	7.73
Cu-3	− 0.02767	6.22	7.25
Cu-4	− 0.02743	6.09	7.13
Cu-5	− 0.01516	7.95	8.70

3.2 Morphological and compositional study

3.2.1 SEM analysis

Figure 2a–f shows SEM micrographs of pristine SnO_2 and Cu-doped SnO_2 samples. SEM images overall exhibit globular morphology form over entire area of substrate. The diameter of these globes like structures is found to be in the range ∼ 0.5 to 1.5 μm. The average grain size of all the samples is calculated by using the SEM micrographs. The values of the average grains size are listed in Table 3.

There is an interesting pattern in the variation of grain size with the doping concentration of Cu. As compared to pristine SnO_2, the grain size of Cu-1 is much larger. With the further increase in doping concentration, the grain size goes on decreasing till Cu-4; but when coping concentration further increased to Cu-5 the grain size is found to increase considerably. This can be explained with the same logic as the variation of crystallite size with doping concentration is explained. When the doping concentration is very low as in Cu-1, very little Cu goes into the lattice of SnO_2 and most of it forms thin films on the grain boundaries resulting into the larger grain size as observed. With the further increase in doping concentration much of the Cu goes into the SnO_2 lattice and very less remains on the grain boundary and hence the grain size goes on decreasing. When doping concentration is increased from Cu-4 to Cu-5, the solubility limit of Cu in SnO_2 lattice is exceeded and hence CuO has tendency of forming layers on the grain boundaries instead of going into the crystal lattice. Al this is clearly visible from the values of grain size as shown in Table 3.

Furthermore, the elemental composition of the pristine and Cu-doped SnO_2 thin films was confirmed using EDX analysis. The corresponding EDX spectra are shown in Fig. 3a–f. In the doped sample, the peak corresponding to Cu is observed which confirms the incorporation of Cu ion into SnO_2 lattice.

3.2.2 TEM analysis

Figure 4 shows TEM and HRTEM images of sample Cu-4. The figure clearly shows the planes of SnO_2 and CuO and the interface between them. The d spacing for SnO_2 and CuO obtained from HRTEM are 0.233 A and 0.180 A, respectively. The corresponding planes for SnO_2 and CuO are found to be (200) and (112), respectively.

3.3 Optical study

The optical property of pristine SnO_2 and Cu-doped SnO_2 thin films was investigated using UV–visible spectroscopy shown in Fig. 5. The UV–visible spectrum of pristine SnO_2 shows a sharp absorption edge around 360 nm, as the Cu concentration increases, the absorption edge gets shifted to higher wavelength over the ultraviolet region. This red shift of absorption edge may be attributed to charge transfer from the valence band of SnO_2 to energy level of copper ions that are located just below the band of SnO_2 [27]. The absorption spectra of the pristine SnO_2 and Cu-doped SnO_2 films were processed to deduce quantitative estimation of optical band gap energy (E_g) using the following Eq. (2), by plotting square of optical absorption coefficient versus photon energy (Tauc plot), and extrapolating a linear section to photon energy axis shown in Fig. 6.

$$(\alpha h\vartheta)^2 = A(h\vartheta - E_g), \tag{2}$$

where α is absorption coefficient, A is a constant, υ is the photon frequency and E_g is band gap energy. The obtained band gap value for pristine SnO_2 is 3.52 eV whereas for Cu-1, Cu-2, Cu-3, Cu-4 and Cu-5, the values are found to be 3.38, 3.30, 3.21, 3.12 and 3.00 eV, respectively. Li et al. reported that, the passivated impurity band of Cu ions occurs in the band gap as there is an existence of compensated donor–acceptor complexes, as a result of it, the band gap of Cu-doped SnO_2 thin films becomes narrower [28].

3.4 Gas-sensing studies

The gas-sensing characteristics of pristine SnO_2 and Cu-doped SnO_2 thin films were investigated in the temperature range from room temperature to 300 °C, towards H_2S gas. The responses of all the sensors are evaluated using change in resistance due to presence of gas and air. It is well known that, the response of the sensor is strongly influenced by the amount of doping and operating temperature [29]. The incorporation of Cu in the SnO_2 lattice causes an increase in oxygen ion vacancies which results in decrease in conductivity of doped SnO_2 sensors [21]. Hence, the Cu-doped SnO_2 films show higher electrical resistance than the pristine SnO_2 films. The optimum
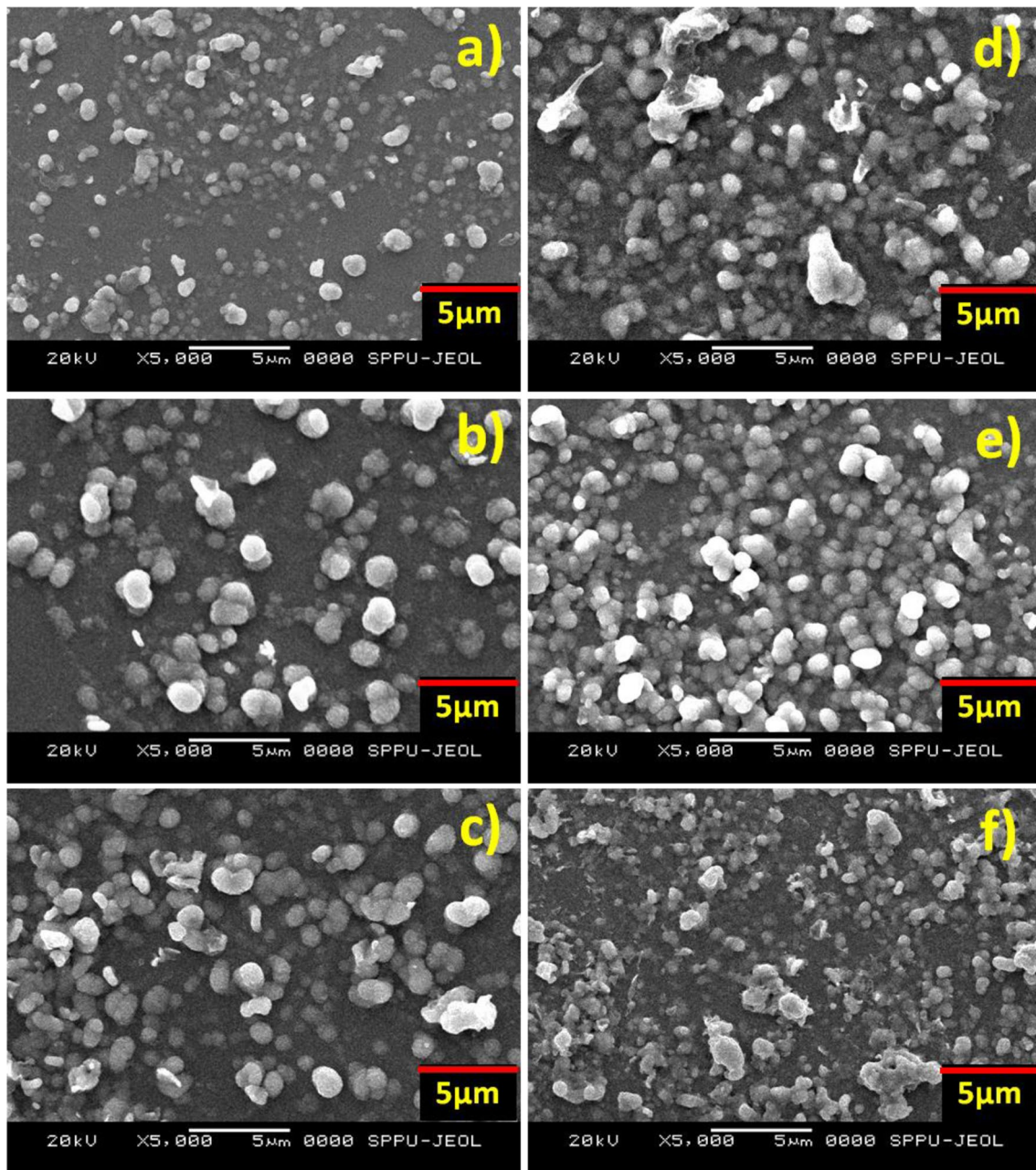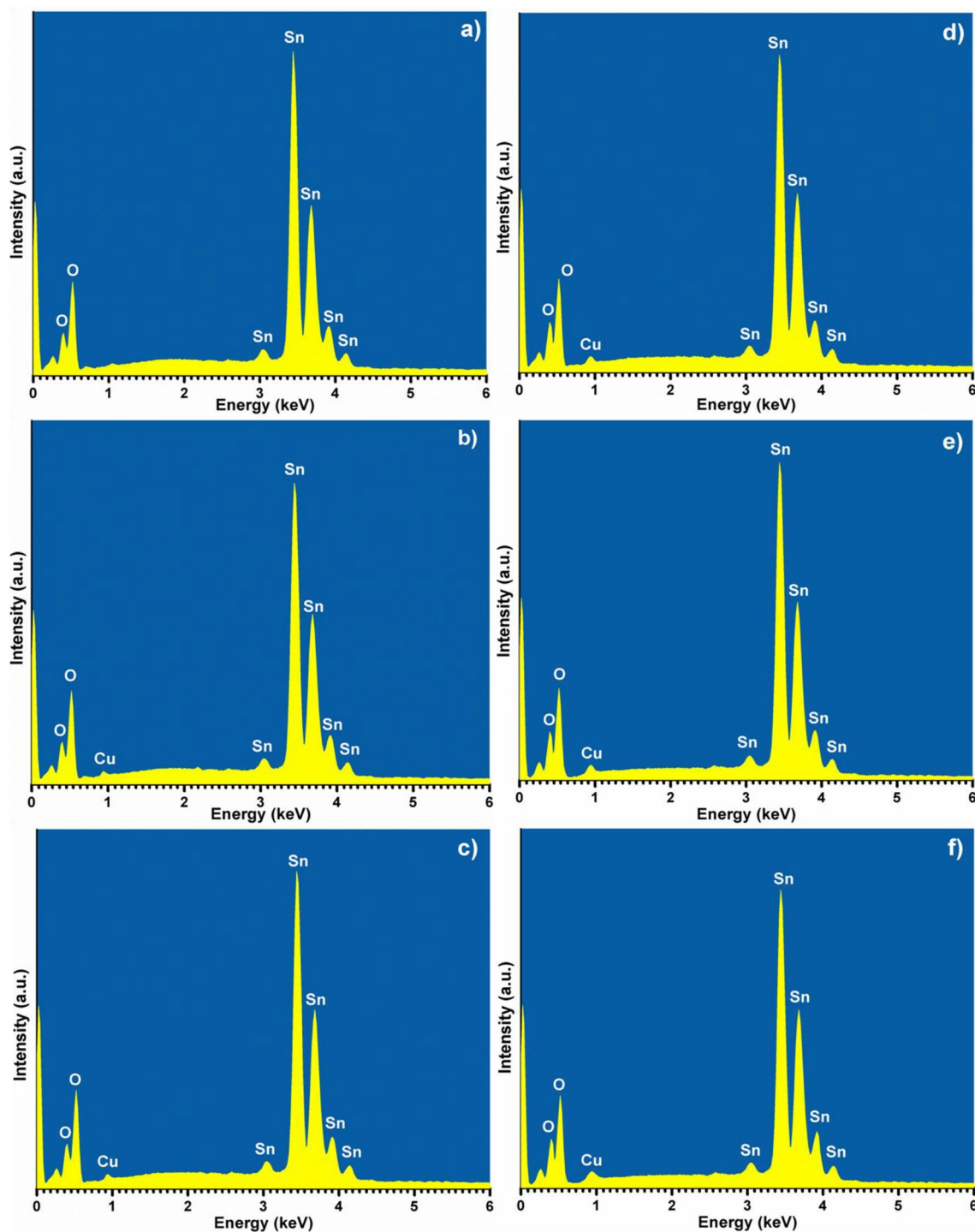
Fig. 2 Typical SEM image of pristine SnO$_2$ and Cu-doped SnO$_2$ **a** SnO$_2$, **b** Cu-1, **c** Cu-2, **d** Cu-3, **e** Cu-4, **f** Cu-5 films

Table 3 Average grain size of the pristine SnO$_2$ and Cu-doped SnO$_2$ samples

Sample	Pristine SnO$_2$	Cu-1	Cu-2	Cu-3	Cu-4	Cu-5
Average grain size (µm)	0.8427	1.0302	0.9916	0.8535	0.7656	0.9028

amount of dopant and operating temperature for pristine SnO$_2$, Cu-1, Cu-2, Cu-3, Cu-4 and Cu-5 is determined by evaluating the response (S) of a sensor as a function of operating temperature for 300 ppm of H$_2$S gas which is depicted in Fig. 7. It can be clearly observed that the responses of the all sensors increase with the increase in temperature and reached to maximum at 150 °C except pristine SnO$_2$ (Max. response at 200 °C) and then goes on decreasing with further increase in temperature. The adsorption and desorption of gas molecules on the surface of sensor due to kinetics of chemical reactions could be the reason behind such behavior of sensor response [30].

Fig. 3 EDX analysis of as-synthesized pristine SnO_2 and Cu-doped SnO_2 **a** SnO_2, **b** Cu-1, **c** Cu-2, **d** Cu-3, **e** Cu-4, **f** Cu-5 films

In addition, the speed of chemical reaction and diffusion of the gas molecules on the surface of the metal oxide based sensor are the major factors in deciding response of the sensor. At lower temperature, the speed of chemical reaction on the surface of sensor is limited whereas at higher temperature speed of gas molecule diffusion to the surface is restricted. Therefore, the speed of both the processes balances at certain temperature by providing enough activation energy to facilitate the reaction mechanism, at that point the sensor gives maximum response [31, 32]. The variation in the response curve for different concentrations of Cu-doped sensor (shown in Fig. 7)

Fig. 4 TEM and HRTEM image of sample Cu-4
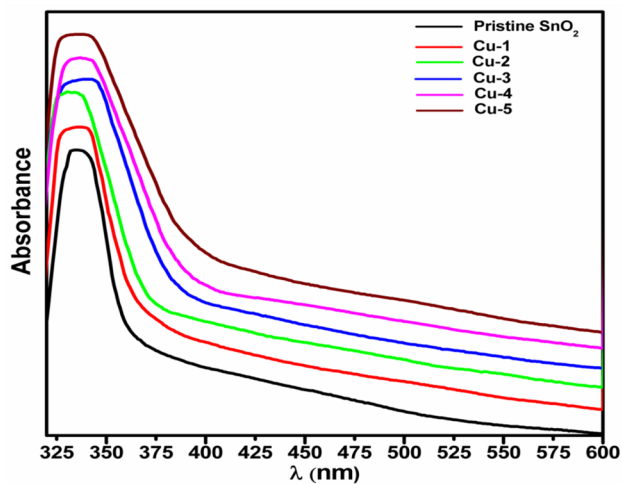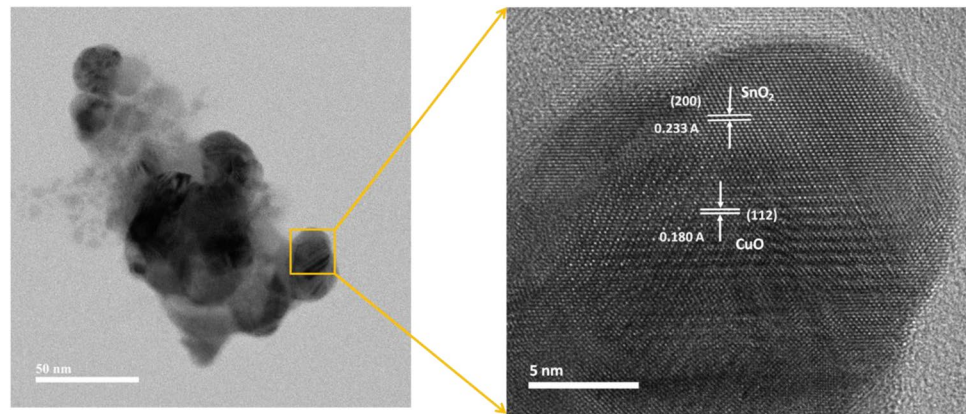
Fig. 5 UV–visible absorption spectra of pristine SnO$_2$ and Cu-doped SnO$_2$ films

leads to believe that, the Cu-dopant favors increase in response of the doped samples due to adsorption of oxygen molecule from atmosphere on the surface of sensor comprised of smaller crystallite size of more sensing cites. In present case, it is observed that the pristine SnO$_2$ sensor shows poor response than the Cu-doped SnO$_2$ sensors and maximum response (S) for the Cu-doped SnO$_2$ sensors is achieved at optimal operating temperature of 150 °C. It specifies that, the operating temperature and concentration of dopant influence the response of the sensor. Particularly, Cu-4 sensor shows maximum response (S) of 63.5% at temperature of 150 °C and is chosen for the further investigation of gas-sensing properties.

For the application point of view, the cyclic test (response/recovery cycles) of several cycles of sensor with different concentration of gas is regarded to be pivotal parameter. Therefore, the cyclic test of Cu-4 sensor is performed at 150 °C. The variation in resistance as function of H$_2$S gas concentration ranging from 50 to 300 ppm is recorded and depicted in Fig. 8. It is observed that, the resistance of the sensor decreases upon injection of H$_2$S gas and reverts back to its original value in presence of air, which indicates n-type behavior of sensing material with good repeatability and stability. Moreover, response and recovery time of the sensor are reckoned as a crucial factor for evaluating performance of the gas sensor. The response and recovery times of pristine SnO$_2$ and Cu-4 sensor are presented in Fig. 9. It has been observed that, Cu-4 sensor exhibits response and recovery time of 15 s and 95 s, respectively, which is found to be superior to pristine SnO$_2$ (59 s and 108 s). Also, the obtained value of response and recovery time for Cu-4 sensor is superior to earlier reported literature [33, 34].

3.5 Gas-sensing mechanism

The gas-sensing mechanism of metal-oxide semiconductor-based gas sensor is mainly based on the change of electrical resistance due to interaction of oxygen and target gas molecules adsorbed or desorbed on the surface of the sensing material and the catalytic activity of dopant [8, 27, 29]. The oxygen molecules are chemisorbed on the surface of SnO$_2$ and Cu-4 sensor when exposed to ambient atmosphere. These oxygen molecules extract an electron from the conduction band of the sensors' surface by forming oxygen ion species (O_2^-, O^- and O^{2-}). Therefore, the carrier concentration at the surface of sensor decreases as more electrons are extracted from the sensor surface by absorbed oxygen which in turn results into increase in electrical resistance of the sensor [29]. At lower operating temperature such as below 100 °C, O_2^- form of oxygen ion dominates due to lower activation energy, on the other hand at higher temperature 100–300 °C, O^- form dominates [24]. In the present study operating temperature range is from RT to 300 °C, O_2^- and O^- ionic species are adsorbed on the surface of sensor and act as active sites which are responsible for the gas-sensing mechanism. The processes are described by following reactions [35]:
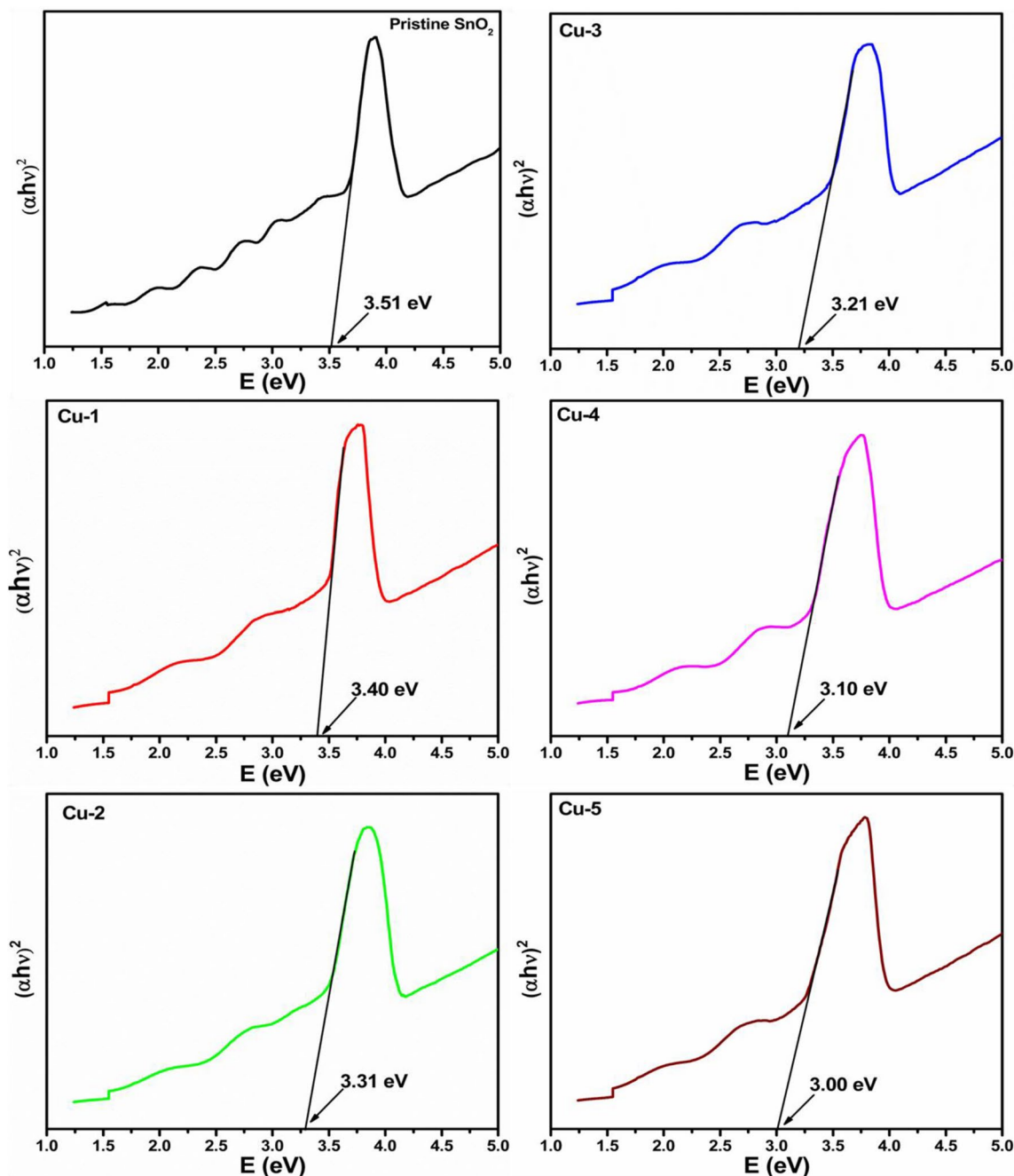
Fig. 6 Tauc plot for pristine SnO_2 and Cu-doped SnO_2 films

$$O_2(air) \rightleftharpoons O_2(ads), \tag{3}$$

$$O_2(ads) + e^- \rightleftharpoons O_2^-(ads), \tag{4}$$

$$O_2^-(ads) + e^- \rightleftharpoons 2O^-(ads). \tag{5}$$

Due to the adsorption of atmospheric oxygen, the space-charge layer is formed at the grain boundaries owing to charge transfer process between adsorbed oxygen ion species

and SnO_2 surface. It is earlier reported that, an electric field is generated at surface due to the net charge; as result of it, the upward band bending is observed. Hence, the Fermi level is shifted into the band gap towards the valance band [19]. All these processes are results in increase in resistance of the sensor. When the sensor is exposed in reductive gas such as H_2S, it reacts with the adsorbed oxygen ionic species and release an electron to the conduction band of sensor surface which leads to increase in electron concentration and
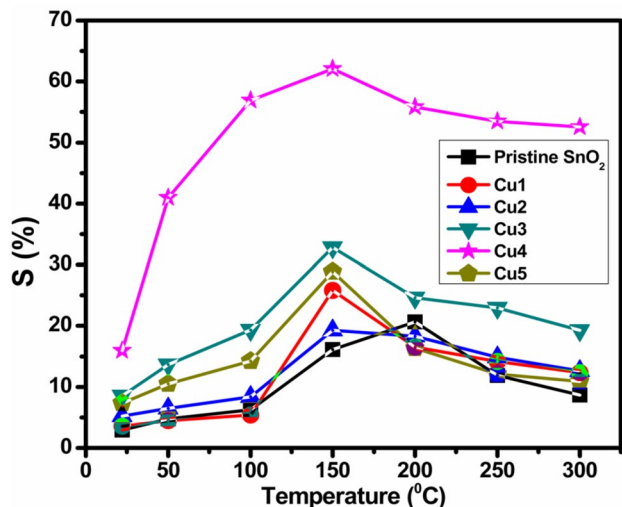
Fig. 7 Response as function of operating temperature (room temperature—300 °C) plot for SnO$_2$ and Cu-doped SnO$_2$ towards 300 ppm H$_2$S gas
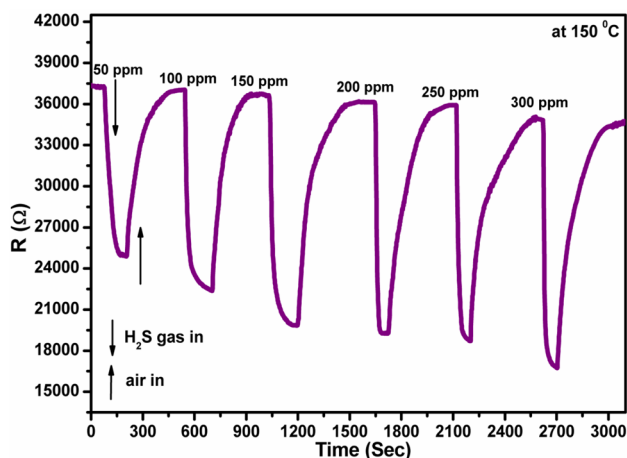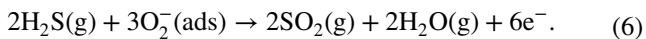

Fig. 8 Plot of response as a function of gas concentration recorded at operating temperature of 150 °C for Cu-4 sensor

carrier mobility [36], resulting into decrease in resistance following the given Eq. (6):

$$2H_2S(g) + 3O_2^-(ads) \rightarrow 2SO_2(g) + 2H_2O(g) + 6e^-. \qquad (6)$$

In present communication, there is an enhancement in response for Cu-doped SnO$_2$ sensor which can be attributed to Cu doping itself. It is well known that, the Cu doping may form CuO when subjected to heat treatment [29]. Moreover, the Cu doping atom has been turned into CuO when entering SnO$_2$ lattice reported by Zhang et al. [37]. Surface of the sensor therefore, consists of numerous CuO–SnO$_2$ p–n junctions. Due to strong electronic interaction between p-type CuO and n-type SnO$_2$, the sensor
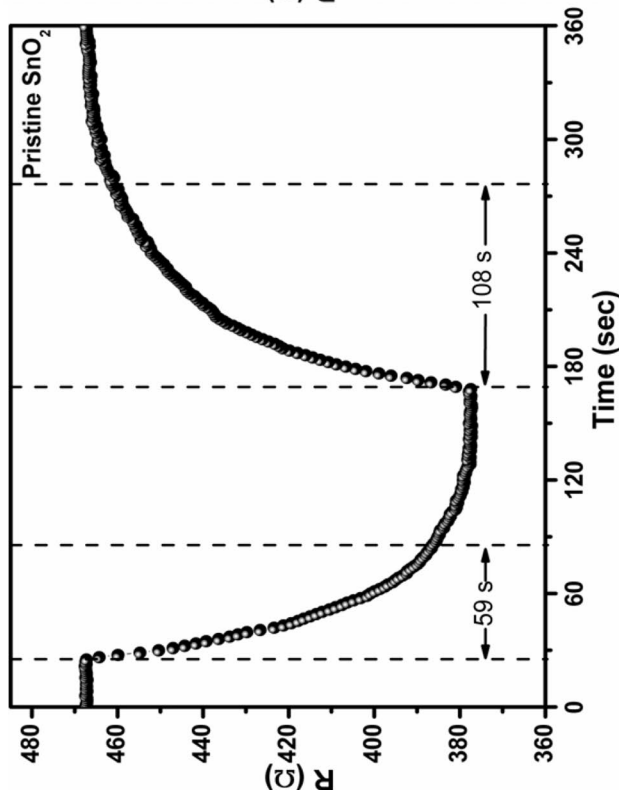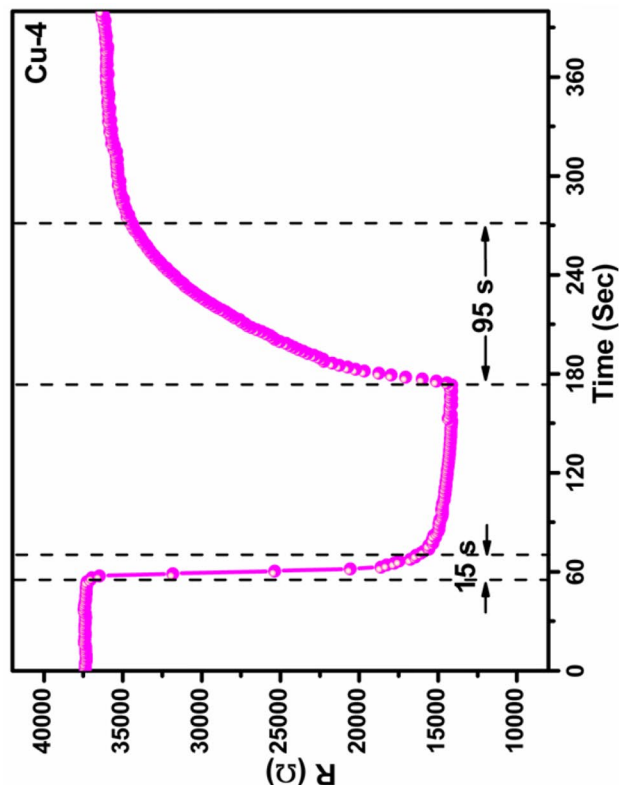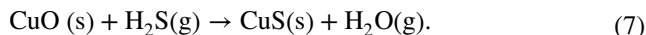

Fig. 9 Response and recovery time curve for pristine SnO$_2$ and Cu-4 sensor at 200 °C and 150 °C temperature, respectively

shows very high resistance. When the sensor is exposed to H_2S gas, CuO is converted to CuS [38], which is metallic in nature with a good electrical conductivity, following reaction (7):

$$CuO\ (s) + H_2S(g) \rightarrow CuS(s) + H_2O(g). \tag{7}$$

Due to the injection of H_2S gas in the surroundings of Cu-doped sensor, the electronic interactions between the $CuO–SnO_2$ junctions are interrupted and leading to a drastic decrease in the electrical resistance. Since, CuS have lower work function than SnO_2, therefore the band bends downward due to which the electrons flow easily [39]. Hence the resistance of sensor drops down drastically in H_2S ambience, as a result of this the Cu-doped sensor exhibits better response compared to pristine SnO_2 (Fig. 7). When the air is introduced into the chamber the oxidation reaction takes place and CuS is converted back to CuO shown in following reaction (8):

$$2CuS\ (s) + 3O_2(g) \rightarrow 2CuO(s) + 2SO_2(g). \tag{8}$$
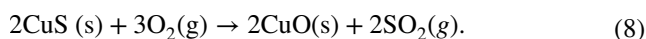
As a result of reaction (8), the electronic interactions between $CuO–SnO_2$ p–n junctions recover and consequently resistance of the sensor is also recovered. Moreover, Kumar et al. [40] reported that, the substitution of Cu^{2+} ion onto Sn^{4+} site could be responsible to produce oxygen vacancies for maintaining charge neutrality, due to which the sensor shows high response. Moreover, the excessive doping may limit the gas-sensing performance of the sensor which is reported in a literature [41].

As discussed in XRD and SEM analysis in sections, it is evident that for sample Cu-4 maximum Cu^{2+} ions enter into the lattice and substitute Sn^{4+} ions. This results in the oxygen vacancies which might cause the increase in active sites. The maximum gas response of Cu-4 can be attributed to this increase in the number of active sites. In case Cu-5, due to the excessive amount of Cu doping in SnO_2 the solubility limit of Cu in SnO_2 is exceeded and hence there is possibility of formation of p-type CuO layers on grain boundaries which limits substitution of Sn^{4+} ion by Cu^{2+} ions that leads to reducing in oxygen vacancies. Lower oxygen vacancies lead to less number of active sites on the surface of sensor that results in minimum interaction of gas molecules. Hence the sensor shows poor response for excessive doping of Cu. Therefore, in present report, due to the optimum amount of Cu doping, Cu-4 sensor shows maximum response as well as short response and moderate recovery time compared to pristine SnO_2. However, these findings are still somewhat speculative and further study is needed to validate them and to improve the sensor performance of Cu-doped SnO_2 sensors.

4 Conclusion

In summary, pristine SnO_2 and Cu-doped SnO_2 globular structured thin films have been synthesized using automotive spray pyrolysis technique. The XRD study shows that, the diffraction peaks of Cu-doped SnO_2 thin film are shifted to higher diffraction angle comparing to pristine SnO_2 due to substitution of Cu^{2+} ions onto Sn^{4+} ions, leading to lattice deformation and increase in oxygen vacancies which are considered as active sites for gas sensing. The UV–visible spectroscopy analysis reveals that, there is an existence of compensated donor–acceptor complexes due to Cu doping and therefore, the band gap of Cu-doped SnO_2 thin films becomes narrower. The possible gas-sensing mechanism of Cu-doped SnO_2 for H_2S gas has been proposed based on adsorption or desorption of air/target gas molecule, catalytic activity of Cu dopant and formation of $CuO–SnO_2$ p–n junction. The Cu-4 sensor exhibits maximum gas response compared to other due to the optimum amount of Cu dopant in SnO_2 is also discussed. The high gas response as well as low response and recovery time shown by Cu-4 (6 mol% Cu-doped SnO_2) sensor could make it potential candidate for H_2S gas sensor.

References

1. S. Das, V. Jayaraman, Prog. Mater Sci. **66**, 112–255 (2014)
2. W. Tian, H. Lu, L. Li, Nano Res. **8**(2), 382–405 (2015)
3. H.J. Snaith, C. Ducati, Nano Lett. **10**(4), 1259–1265 (2010)
4. L.Y. Jiang, X.L. Wu, Y.G. Guo, L.J. Wan, J. Phys. Chem. C **113**(32), 14213–14219 (2009)
5. X. Fang, J. Yan, L. Hu, H. Liu, P.S. Lee, Adv. Funct. Mater. **22**(8), 1613–1622 (2012)
6. C.S. Moon, H.R. Kim, G. Auchterlonie, J. Drennan, J.H. Lee, Sens. Actuators B: Chem. **131**(2), 556–564 (2008)
7. S. Xu, K. Kan, Y. Yang, C. Jiang, J. Gao, L. Jing, P. Shen, L. Li, K. Shi, J. Alloy Compd. **618**, 240–247 (2015)
8. P.S. Kolhe, P.M. Koinkar, N. Maiti, K.M. Sonawane, Phys. B Cond. Matter **524**, 90–96 (2017)
9. D.C. Dorman, F.J.M. Moulin, B.E. McManus, K.C. Mahle, R.A. James, M.F. Struve, Toxicol. Sci. **65**(1), 18–25 (2002)
10. N. Bhardwaj, A. Pandey, D.K. Avasthi, S. Mohapatra, J. Alloys Compd. **680**, 155–162 (2016)
11. J. Zhang, X. Liu, S. Wu, M. Xu, X. Guo, S. Wang, J. Mater. Chem. **20**(31), 6453–6459 (2010)
12. W.J. Moon, J.H. Yu, G.M. Choi, Sens. Actuators B Chem. **87**(3), 464–470 (2002)
13. L. Liu, Y. Zhang, G. Wang, S. Li, L. Wang, Y. Han, X. Jiang, A. Wei, Sens. Actuators B Chem. **160**(1), 448–454 (2011)
14. X. Liu, J. Zhang, X. Guo, S. Wu, S. Wang, Sens. Actuators B Chem. **152**(2), 162–167 (2011)

15. Y.C. Lee, H. Huang, O.K. Tan, M.S. Tse, Sens. Actuators B Chem. **132**(1), 239–242 (2008)
16. N.S. Ramgir, I.S. Mulla, K.P. Vijayamohanan, Sens. Actuators B Chem. **107**(2), 708–715 (2005)
17. W. Wei, Y. Dai, B. Huang, J. Phys. Chem. C **115**(38), 18597–18602 (2011)
18. N. Bhardwaj, A. Pandey, B. Satpati, M. Tomar, V. Gupta, S. Mohapatra, Phys. Chem. Chem. Phys. **18**(28), 18846–18854 (2016)
19. R.K. Mishra, A. Kushwaha, P.P. Sahay, RSC Adv. **4**(8), 3904–3912 (2014)
20. L. Liu, T. Zhang, L. Wang, S. Li, Mater. Lett. **63**(23), 2041–2043 (2009)
21. C.M. Ghimbeu, M. Lumbreras, M. Siadat, R.C. van Landschoot, J. Schoonman, Sens. Actuators B Chem. **133**(2), 694–698 (2008)
22. N. Bhardwaj, S. Mohapatra, Ceramics Inter. **42**(15), 17237–17242 (2016)
23. S.S. Roy, J. Podder, J. Optoelectr. Adv. Mater. **12**(7), 1479 (2010)
24. P.S. Kolhe, A.B. Shinde, S.G. Kulkarni, N. Maiti, P.M. Koinkar, K.M. Sonawane, J. Alloy Compd. **748**, 6–11 (2018)
25. S.K. Sinha, R. Bhattacharya, S.K. Ray, I. Manna, Mater. Lett. **65**(2), 146–149 (2011)
26. A. Johari, S. Srivastav, M. Sharma, M.C. Bhatnagar, J. Magn. Magn. Mater. **362**, 1–6 (2014)
27. W.B. Soltan, M. Mbarki, S. Ammar, O. Babot, T. Toupance, Opt. Mater. **54**, 139–146 (2016)
28. Y. Li, R. Deng, Y. Tian, B. Yao, T. Wu, Appl. Phys. Lett. **100**(17), 172402 (2012)
29. W.X. Jin, S.Y. Ma, Z.Z. Tie, J.J. Wei, J. Luo, X.H. Jiang, T.T. Wang, W.Q. Li, L. Cheng, Y.Z. Mao, Sens. Actuators B Chem. **213**, 171–180 (2015)
30. N. Yamazoe, Sens. Actuators B Chem. **5**(1–4), 7–19 (1991)
31. T. Zhang, Y. Zeng, H.T. Fan, L.J. Wang, R. Wang, W.Y. Fu, H.B. Yang, J. Phys. D Appl. Phys. **42**(4), 045103 (2009)
32. S.K. Lim, S.H. Hwang, D. Chang, S. Kim, Sens. Actuators B Chem. **149**(1), 28–33 (2010)
33. A. Khanna, R. Kumar, S.S. Bhatti, Appl. Phys. Lett. **82**(24), 4388–4390 (2003)
34. A. Chowdhuri, S.K. Singh, K. Sreenivas, V. Gupta, Sens. Actuators B Chem. **145**(1), 155–166 (2010)
35. M. Zhao, X. Wang, L. Ning, J. Jia, X. Li, L. Cao, Sens. Actuators B Chem. **156**(2), 588–592 (2011)
36. K. Wang, T. Zhao, G. Lian, Q. Yu, C. Luan, Q. Wang, D. Cui, Sens. Actuators B Chem. **184**, 33–39 (2013)
37. S. Zhang, P. Zhang, Y. Wang, Y. Ma, J. Zhong, X. Sun, ACS Appl. Mater. Int. **6**(17), 14975–14980 (2014)
38. A. Tang, S. Qu, K. Li, Y. Hou, F. Teng, J. Cao, Y. Wang, Z. Wang, Nanotechnology **21**(28), 285602 (2010)
39. X. Xue, L. Xing, Y. Chen, S. Shi, Y. Wang, T. Wang, J. Phys. Chem. C **112**(32), 12157–12160 (2008)
40. V. Kumar, S. Sen, K.P. Muthe, N.K. Gaur, S.K. Gupta, J.V. Yakhmi, Sens. Actuators B Chem. **138**(2), 587–590 (2009)
41. P. Mohanapriya, H. Segawa, K. Watanabe, K. Watanabe, S. Samitsu, T.S. Natarajan, N.V. Jaya, N. Ohashi, Sens. Actuators B Chem. **188**, 872–878 (2013)